Journal of Materials Chemistry A RSCPublishing

Article

Cite this: DOI: 10.1039/x0xx00000x

Received 00th January 2012, Accepted 00th January 2012

DOI: 10.1039/x0xx00000x

www.rsc.org/

Polymorphisms and morphological studies of a difluorobenzothiadiazole conjugated copolymer with 7.8% Polymer Solar Cells Efficiency

Chi-Feng Huang,[a] Jen-Yun Chang,[a] Sin-Hong Huang, [a] Kuan-Yi Wu, [a] Jyun-Fong Jheng, [a] Wei-Tsung Chuang, [b] Chain-Shu Hsu, [a] and Chien-Lung Wang, [a] *

This study presents the structural characterizations of a 5,6-difluorobenzo-2,1,3-thiadiazole (FBT) – quaterthiophene (Th_4) alternating copolymer (PTh_4FBT) and how the crystalline nature of PTh_4FBT affects the $PTh_4FBT/PC_{71}BM$ morphology and the device performances. The single crystal structure of 5,6-difluoro-4,7-di(thiophen-2-yl)benzothiadiazole (Th_2FBT) first confirms the low conformational preference of the FBT containing molecule. Since crystallization process does not assist to unify the conformation of Th_2FBT, both intrachain conformation and interchain *c*-shifts in the crystalline state of PTh_4FBT have to be scrutinized. Through comparing the 2D WAXS pattern of PTh_4FBT, and the simulated patterns generated from Cerius^2 molecular modeling, it was found that the diffration pattern generated from the lattice containing PTh_4FBT with *anti*-conformation and limited interchain *c*-shift matches best with the experimental one. The face-to-face interchain stacking of PTh_4FBT renders the strong crystalline nature to the polymer and caused large segregation in the $PTh_4FBT/PC_{71}BM$ blend system, which was indicated by the TEM and GI WAXS morphological studies. The aggregation size was reduced via the use of the 1-chloronaphthalene additive. The optimized morphology led to the improved J_{sc} and FF. The single-junction $PTh_4FBT/PC_{71}BM$ based polymer solar cells deliver a high PCE of 7.75 % with V_{oc} of 0.76 V, a J_{sc} of 14.36 mA/cm^2, and a FF of 71.0 %.

Introduction

The developments of donor (D)-acceptor (A) conjugated copolymers have brought significant enhancements in the performances of bulk-heterojunction (BHJ) polymer solar cells (PSCs) and organic field-effect transistors (OFETs).[1-9] In these applications, the molecular properties of polymers, including the highest occupied molecular orbital level (E_{HOMO}), the lowest unoccupied molecular orbital level (E_{LUMO}), and the intrinsic bandgap (E_g), together with the solid state morphology determine the output performances.

Main structural units in conjugated polymers, such as thiophene, cyclopentadithiophene (CDT), dithienosilole (DTS), benzothiadiazole (BT), thienopyrrole-dione (TPD), etc…, possess two-fold rotational symmetry perpendicular to the polymer backbone, but lack symmetry along the backbone. Consequently, the rotation of the structural units will change the conformations and the spatial arrangements of the polymers,[10] and allow the polymers to switch between different physical states. Compared to poly(3-hexylthiophene), D-A conjugated copolymers possess more complex main-chain structures, and in most cases, have much bulkier branch alkyl side chains. These molecular characteristics increase the difficulty for the polymers to interact intermolecularly, and to pack orderly. However, many D-A conjugated polymers actually formed highly order lamellar structures and show higher phase stability than poly(3-hexylthiophene).[9,11-15] Therefore, the origins of the highly crystalline nature of the D-A copolymers are intriguing and worthwhile to be explored.

Parameters in the solid-state structures of a conjugated polymer largely include backbone conformations, interchain π-stacking distances, and degrees of longitudinal shifts (*c*-shift).[16] These parameters strongly affect the backbone geometries,[17-23] electronic structures,[10] and intermolecular transfer integrals[24] of the D-A copolymers, which subsequently influence the device performances.[25-29] Currently, these solid-state parameters have been studied in only limited cases, including the CDT-BT,[9,16] DTS-BT,[30] naphthalene diimide (NDI)-bithiophene[31] copolymers. 5,6-difluorobenzo-2,1,3-thiadiazole (FBT) containing D-A copolymers, such as poly(5,6-difluorobenzo-2,1,3-thiadiazole-4,7-diyl)-alt-(3',4''-di-(2-octyldodecyl)-2,2';5',2'';5'',2'''-quaterthiophene-5,5'''-diyl)} (PTh_4FBT)

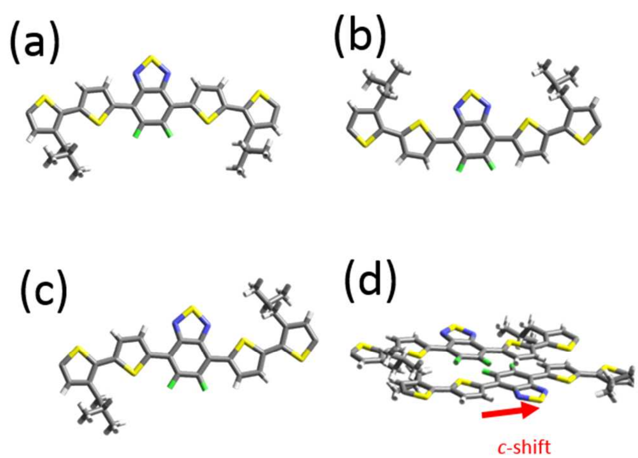

Scheme 1. Three possible conformations of the repeat unit of PTh_4FBT: (a) *syn1*, (b) *syn2*, and (c) *anti* conformation, and (d) the illustration of the degree of *c*-shift.

have been recently reported as a class of conjugated polymers that form highly ordered solid-state structure and delivered excellent device performances.[12, 32] However, studies about the solid-state parameters of the FBT copolymers remains absent, due to the high structural complexity of the conjugated copolymers. The non-fused and extended donor unit, quaterthiophene (Th_4) of PTh_4FBT results in an easier disturbed conjugated backbone, and gives more possible conformation isomers to the repeat units **(Scheme 1a-1c)**. Moreover, theoretical evaluations suggested that the intramolecular CH…F interaction is not strong enough to lock the conformation[10, 33] which also increase the comformational ambiguity in the solid-state. Additionally, both the electrostatic interactions between the D and A units,[16, 34] and the intermolecular A-A interactions [31, 35]can act as the driving forces for the π-π stacking, making the degree of *c*-shift **(Scheme 1d)** in the packing of PTh_4FBT uncertain.

Herein, to address the above issues, crystal structures of 5,6-difluoro-4,7-di(thiophen-2-yl)benzo-2,1,3-thiadiazole (Th_2FBT) and PTh_4FBT were investigated. The single crystal structure of Th_2FBT confirmed the presence of conformational disorder in the crystalline state (**Figure 1**). When viewing along the π-stacking direction (**Figure 2**), the FBT units stack parallel with a *c*-shift of 3.38 Å. The conformational disorder of Th_2FBT makes it necessary to consider the conformational isomers of PTh_4FBT. Therefore, three possible conformations - *syn-1*, *syn-2* and *anti*, showing in **Scheme 1** were considered in the structural characterizations of PTh_4FBT. The two-dimensional wide angle X-ray scattering (2D WAXS) pattern of PTh_4FBT revealed that PTh_4FBT adopts the *anti* conformation. Furthermore, the FBT units stack cofacially with zero *c*-shift, possibly due to the preferable intermolecular A-A interactions.

For BHJ PSCs, morphological optimization of the polymer/PCBM blend thin films is critical in reaching high performances.[36] In general, the formation of large segregation domains was mainly attributed to the PCBM crystallization.[29, 37-39] Processing additives, such as 1,8-diiodooctane (DIO), 1-chloronaphthalene (1-CN) were thus required to, on the one hand, inhibit the PCBM crystallization, and on the other, enhance the polymer crystallinity. PTh_4FBT has strong crystallization tendency. An interesting question raised with the enhanced crystallization tendency is that whether or not the polymer crystallization will overwhelm the PCBM crystallization, and dominate the phase separation in the polymer/PCBM thin film. In previous studies, although CDT-BT, DTS-BT, and NDI-Th_2 D-A copolymers also show strong crystalline nature and packed into highly ordered structures,[9,16,30,31] the segregation phenomenon of these polymers in the polymer/PCBM thin film was less investigated. The grazing incidence wide-angle X-ray scattering (GI WAXS) and transmission electron microscopy (TEM) observations of the $PTh_4FBT/PC_{71}BM$ thin films revealed that instead of $PC_{71}BM$, PTh_4FBT crystallized and segregated into large domain in the $PTh_4FBT/PC_{71}BM$ thin films. Thus, morphological optimization was reached via diminishing the crystallization of the PTh_4FBT via the addition of 8 v% 1-CN. The optimized morphology led to the elevated J_{sc} and FF, and pushed up the PCE to 7.75 % in the single junction $PTh_4FBT:PC_{71}BM$ inverted PSCs.

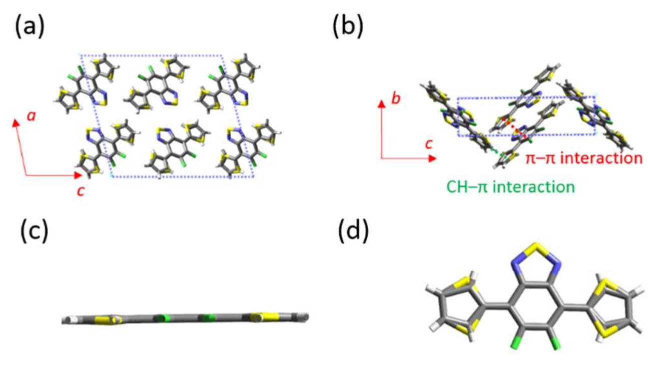

Figure 1. (a) *ac* plane and (b) *bc* plane projections of the molecular packing of Th_2FBT molecules in the unit cell; (c) side view and (d) top view of the individual Th_2FBT in the unit cell.

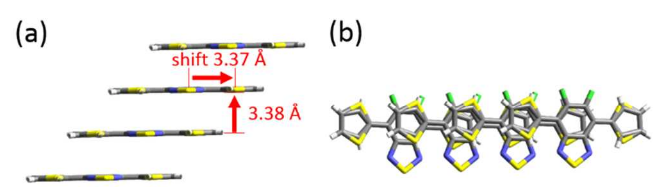

Figure 2. (a) Side view and (b) top view of the π-stacking of four Th_2FBT molecules.

Experimental Section

Single Crystal X-ray Diffraction and Structure Analysis of Th_2FBT. Th_2FBT was dissolved in solvent (0.5 mg mL^{-1}) with dichloromethane and methanol (Volume % 1:2). The single crystal of Th_2FBT was obtained by slow evaporation of dichloromethane and methanol solution (Volume % 1:2) at a room temperature. The diffraction measurements were carried out using Oxford Gemini Duo system single-crystal X-ray diffractometer equipped with Cryojet with wave length 1.54 Å at 200 K. Unit cell parameters were determined by least-squares refinement of the three-dimensional centroids of several thousand reflections. The structure was solved by direct method with SHELXS-97 and refined using full-matrix least-squares on F^2.

2-D fiber X-ray diffraction Measurements. PTh_4FBT fiber sample was prepared by extruding the sample from a homemade stainless steel extruder at ca. 210 °C. The 2D WAXS pattern of PTh_4FBT fiber was collected at the BL17A1 beamline of the National Synchrotron Radiation Research Center (NSRRC) in Taiwan. The wavelength of the incident X-rays was 1.33 Å, delivered from the superconducting wavelength-shifting magnet, and a Si (111) double-crystal monochromator. The diffraction pattern was recorded at room temperature with a Mar345 imaging plate detector approximately 300 mm from sample positions and typical exposure duration 5 minutes. The pixel size of Mar345 is 100 µm. The pattern was taken at room temperature with the x-ray incident beam perpendicular to the shear direction.

Molecular Packing and Crystallographic Simulation. Molecular packings of PTh_4FBT and simulated fiber diffraction patterns were performed by using the software package Cerius[2]. Basic unit cell parameters determined by analysis of 2D WAXS pattern of PTh_4FBT were used to build the unit cell. The basic structures and conformations of the PTh_4FBT repeat unit were constructed based on the coplanar geometry of Th_2FBT solved from the single crystal diffraction result. The built lattices containing controlled variables including: conformations (*syn1*, *syn2*, and *anti*) and the degree of *c*-shift. By comparing the simulated diffractions with the experimental one, the best fitting lattice model was determined.

BHJ PSC Fabrication and Characterization. The device structure of the inverted PSC is ITO/ZnO/PTh_4FBT: $PC_{71}BM$ /MoO_3/Ag. The ITO glass substrates were cleaned with detergent, deionized water, acetone, and isopropyl alcohol in an ultrasonic bath and then dried overnight in an oven at >100 °C. Zinc acetylacetonate hydrate (purchased from Aldrich) dissolved in methanol (20 mg mL^{-1}) was spin-casted on pre-cleaned ITO substrates and baked at 130 °C for 10 minutes in the air to form the ZnO layer with thickness of 30 nm. 10 mg PTh_4FBT were dissolved in solution of 920 µL ODCB and 80 µL 1-chloronaphthalene (Volume % = 92:8), and then 10 mg $PC_{71}BM$ (purchased from Nano-C) was added into the solution. The solution was stirred at 100 °C in glove box for overnight, filtrated through a 0.45 um filter, and then spin-coated onto the ZnO layer at 600 rpm for 40 sec. After spin-coating, the sample was solvent annealed in the ODCB atmosphere for 2 hours and then annealed at 80 °C for 15 minutes. The anode made of MoO_3 (6 nm) and Ag (150 nm) was evaporated through a shadow mask under vacuum ($<10^{-6}$ Torr). Each sample consists of four independent pixels defined by an active area of 0.04 cm^2. The devices were encapsulated and characterized in air under 100 mW/cm^2 AM 1.5 simulated light measurement (Yamashita Denso solar simulator). Current−voltage (*J*−*V*) characteristics of PSC devices were obtained by a Keithley 2400 SMU. Solar illumination conforming the JIS Class AAA was provided by a SAN-EI 300W solar simulator equipped with an AM 1.5G filter. The light intensity was calibrated with a Hamamatsu S1336-5BK silicon photodiode.

Grazing incidence wide-angle X-ray scattering (GI WAXS). Si (100) wafers were cleaned by sonication in acetone and isopropyl alcohol before a 20 min UV-ozone treatment, and it was used as the substrates for the GI WAXS measurements. Solution 1 was prepared by dissolving 10 mg PTh_4FBT and 10 mg $PC_{71}BM$ (wt % 1:1) in 920 µL of ODCB and 80 µL of 1-chloronaphthalene (Volume % = 92:8)); solution 2 was prepared by dissolving 10 mg PTh_4FBT and 10 mg $PC_{71}BM$ in 1ml ODCB. Both solutions were stirred at 100 °C for overnight. The thin film with and without 1-CN were prepared by spin-casting solution 1 and 2 onto the Si substrate at 600 rpm for 40 sec. Then, samples of the thin film were solvent annealed in the ODCB atmosphere for 2 hours and then annealed at 80 °C for 15 minutes. GI WAXS measurements were performed at BL01C2 beamline in NSRRC. The wavelength of the incident X-rays is 1.03Å, which was delivered from the superconducting wavelength-shifting magnet, and monochromized a Si (111) double-crystal. The diffraction pattern was recorded at room temperature with a Mar345 imaging plate detector approximately 454.9 mm from sample positions. The angle between the film surface and the incident beam was fixed at 0.18˚.

Transmission Electron Microscopy (TEM). The thin-film samples for TEM were first spin-coated onto an ITO substrate covered with PEDOT: PSS from solution 1 and 2 at 600 rpm for 40sec and were solvent annealed in the ODCB atmosphere for 2 hours, and then thermal annealed at 80 ° C for 15 minutes. The samples were then immersed into water to dissolve the PEDOT:PSS layer and separate the thin films from the ITO substrate. Thin films floated on a water surface were picked up by copper grids coated with amorphous carbon layer, dried under vacuum six hours, and used in the TEM observations. TEM observations were performed in bright-field mode on a JEOL JEM-2010 transmission electron microscope with an accelerating voltage of 160 kV equipped with a Gatan-831 CCD camera.

Result and Discussion

Single Crystal Structure of Th_2FBT

The low conformational preference of FBT containing molecules although have been theoretically predicted.[10] have not been experimentally proven yet. Thus, the conformational disorder and the intermolecular arrangements of the FBT containing molecule was first studied from the single crystal structure of Th_2FBT. Detailed crystallographic data can be found in **Table S1**. **Figure 1a** and **1b** are the *ac* plane and *bc* plane projections of the unit cell. The packing structure shown in **Figure 1b** indicated that both the π…π and CH…π interactions contribute to the packing of Th_2FBT. In the unit cell, the FBT core of Th_2FBT is nearly coplanar to the flanking 2-thienyl groups (**Figure 1c**). Most importantly, the coexistence of the *syn1*, *syn2* and *anti* conformations (**Scheme S1**) is evidently shown in **Figure 1d**, because the flanking 2-thienyl groups have equal probability pointing toward or opposite to the fluorine substitutions of the FBT core. Therefore, the conformational disorder is present in the crystalline phase of Th_2FBT. Although the intramolecular S…F interaction in the *syn1* conformation,[40] and the CH…F

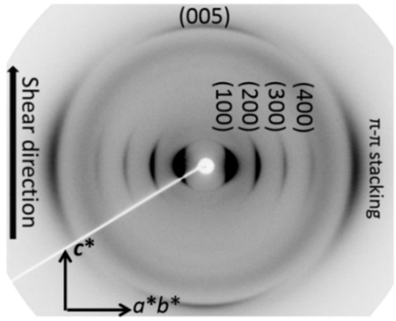

interaction in the *syn2*

Figure 3. 2D WAXS pattern of oriented PTh_4FBT. The shear direction is on the meridian.

conformation were considered as conformational lockers,[41] the crystal structure of Th_2FBT shows that these intramolecular interactions are not sufficient to suppress the conformational disorder. **Figure 2** shows the side view and top view of the π-stacking, the Th_2FBT molecules stack parallel with an intermolecular *c*-shift of 3.38 Å. The 3.38 Å *c*-shift allows the neighboring Th_2FBT molecules to interact not only through the π…π interaction, but also through the CH…π interaction. In addition, it also reduces the steric hindrance among the parallel aligned thiadiazole groups of the FBT cores. The cooperative π…π and CH…π interactions resulted in the final herringbone assembling of the Th_2FBT molecules in the crystalline state as shown in **Figure 1b**.

Molecular modeling of PTh_4FBT

The single crystal structure of Th_2FBT molecule confirmed the low conformational preference of Th_2FBT and the 3.38 Å intermolecular *c*-shift in the crystalline state. The question followed would be whether or not the conformational disorder and *c*-shift remain as the assembling principle in PTh_4FBT where Th_2FBT acts as a structural unit. To know that, the lattice parameters of PTh_4FBT were first deduced from its 2D WAXS pattern, and the molecular packing of PTh_4FBT in the lattice was further investigated through the simulated lattice models and 2D WAXS patterns generated in Cerius^2 software package. As shown in **Scheme 1**, the possible conformations (*syn1*, *syn2*, and *anti*) of the PTh_4FBT repeat unit and the degree of *c*-shift were carefully analyzed in this section.

Figure 3 shows the 2D WAXS pattern of an extruded PTh_4FBT sample. The chain axis (*c*-axis) of PTh_4FBT is aligned along the shear direction. Therefore, the Bragg diffractions along the meridian were used to identify the *c*-dimension, and those along the equator are used to identify the *a*- and *b*-dimensions. In **Figure 3**, the first four equatorial reflections are equally spaced, and at q = 3.08, 6.15, 9.23 and 12.3 nm^{-1}, respectively, indicating the presence of a long-range ordered lamellar structure with *d*-spacing of 2.02 nm. The *a*-dimension was thus assigned to be 2.02 nm and the four diffractions were indexed as the (100), (200), (300) and (400) diffractions. The fifth equatorial diffraction arc is at q = 17.0 nm^{-1} (*d*-spacing of 0.37 nm), representing the periodic π-stacking of PTh_4FBT. To investigate the structural variables shown in **Scheme 1**, the *b*-dimension was set to be twice of the $d_{\pi-\pi}$ (2 × 0.37 nm = 0.74 nm), so that a unit cell will contain 2 repeat units, and the structural variables can be incorporated into the simulated lattice (**Figure 4-5**, *vide infra*).

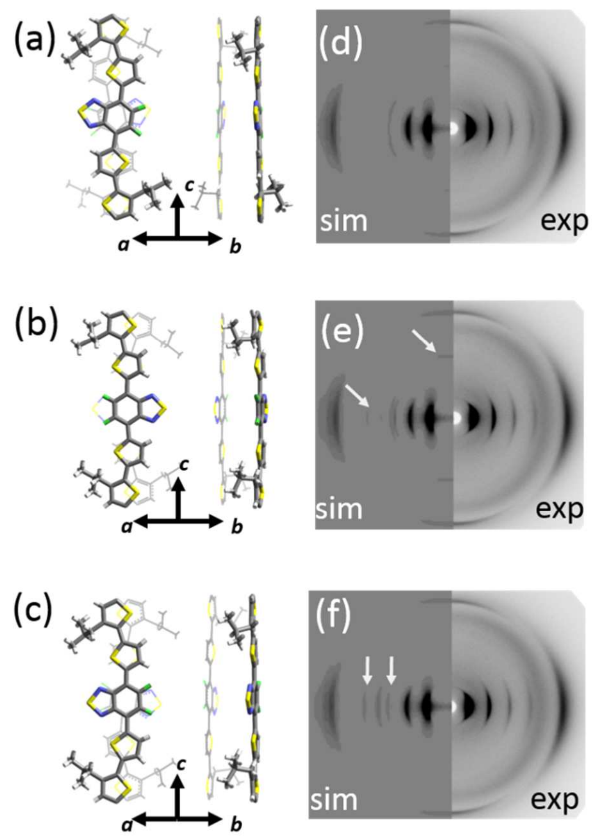

Figure 4. The *ac* and *bc* projections of the models with (a) *anti* conformation, (b) *syn1* conformation, and (c) *syn2* conformation. Left panels of (d)-(f): corresponding simulated 2D WAXS patterns of model (a)-(c).

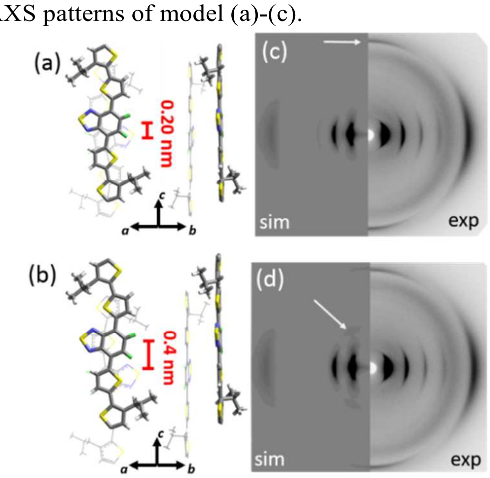

Figure 5. The *ac* and *bc* projections of the models with (a) 0.20 nm *c*-shift and (b) 0.40 nm *c*-shift. Left panels in (c) and (d): simulated 2D WAXS patterns of model (a) and (b).

The meridional arc at $q = 15.7$ nm^{-1} (d-spacing of 0.40 nm) representing the periodicity along the c-axis. The length of a PTh_4FBT repeat unit is around 2 nm, and the repeat unit contains five aromatic units (1 FBT and 4 thienyl units). Since this length is around five times of 0.40 nm, it is reasonable to index the meridional arc as the (005) diffraction, and set the c-dimension as $0.40 \times 5 = 2.00$ nm, which represents the length of one PTh_4FBT repeat unit. The 0.40 nm d-spacing of the (005) diffraction can therefore be regarded as the average distance between the aromatic units along the chain axis. Finally, because the angles between the equatorial (h00), (0k0) diffractions and the meridional (00l) diffraction are both 90^o, the α and β angles can be determined as 90˚. Due to the lack of the (hk0) diffraction, the γ angle cannot be directly deduced from the the 2D WAXS pattern. To give the best assumptiom to the γ angle, the density of the PTh_4FBT was measured. The measured density of the sheared sample was 1.11 g cm^{-3}. By assuming $\gamma = 90$˚, the ordered phase of PTh_4FBT gave a theoretical density 1.14 g cm^{-3}. Because as shown in **Figure S1**, deviating the γ angel from 90˚ will increase the theoretical densities, which further enlarge the differences between the experimental and theoretical densities, the γ was set at 90˚ to give the closest match between the experimental and theoretical densities. Since reaching 100% crystallinity is difficult for polydispersed long-chain molecules, the lower experimental density suggested the presence of amorphous regions in the samples. The lattice parameters of PTh_4FBT are thus $a = 2.02$ nm, $b = 0.74$ nm, $c = 2.00$ nm, and $\alpha = \beta = \gamma = 90$˚. The experimental and calculated diffraction d-spacing values of the crystal lattice are listed in **Table S3**.

The molecular packing of PTh_4FBT were studied via lattice models of PTh_4FBT built by using Cerius^2 software package. The lattice parameters determined in the previous section were used to construct the unit cell, and the structural variables including the conformations (*syn1*, *syn2*, and *anti*) and the degree of c-shift, were built into the lattice models. Simulated 2D fiber WAXS pattern generated from each lattice model was then compared to the experimental one to identify the most plausible packing structure. **Figure 4a-4c** show the lattice models containing repeating units with *anti*, *syn1*, and *syn2* conformations, respectively. The simulated 2D WAXS patterns of the three models are shown in the left panels of **Figure 4d-4f**. The model with *anti* conformation gives a simulated pattern (**Figure 4d**) matches well with the experimental one, while the models with *syn1* and *syn2* conformations provide extra diffractions that cannot be found in the experimental pattern. Increase of the degree of c-shift to 0.20 nm (**Figure 5a**) and 0.40 nm (**Figure 5b**) also generated extra diffraction arcs in the quadrants, and weakened the (005) diffraction on the meridian, as shown in the left panels of **Figure 5c** and **5d**. Therefore, the results suggested that the most probable comforamtion of PTh_4FBT in the solid-state structure is the *anti* conformation. Moreover, the PTh_4FBT chains are stacked cofacially with very small c-shift. It is interesting to find that PTh_4FBT polymer packs differently from that of Th_2FBT molecule, which contain conformational isomers and stacked with c-shift of 3.38 Å. It is speculated that the long-chain structure of PTh_4FBT reduce the contribution of the chain-end CH…π interactions, and the mutliple intermolecular FBT-FBT interactions along the PTh_4FBT chains may dominate the assembling and resulted in the zero c-shift packing.

BHJ PSC Characterizations and Morphological Optimization

The PCE of the PTh_4FBT:$PC_{71}BM$ (1:1, w/w) inverted PSCs was 6.82% with device architecture of ITO/ZnO (30 nm)/PTh_4FBT:$PC_{71}BM$ (95 nm)/MoO_3 (6 nm)/Ag (150 nm) in our previous work.[12] The phase morphology and the phase segregation mechanism of the blend were unclear, and made the morphological optimization difficult. To optimize the morphology, the PTh_4FBT:$PC_{71}BM$ (1:1, w/w) thin film was studied by TEM and GI WAXS. As shown in **Figure 6a**, the TEM image of the PTh_4FBT:$PC_{71}BM$ thin film prepared from the *o*-dichlorobenzene (ODCB) solution clearly show the large dark domains with diameters between 50–140 nm. GI WAXS pattern of the thin film on a silicon wafer prepared in the same condition is shown in **Figure 7a**. The diffractions at $q_z = 3.08$ and 6.15 nm^{-1} corresponds to the (100) and (200) reflections of PTh_4FBT. No reflection from $PC_{71}BM$ was observed. The results indicate that in the blend thin film, PTh_4FBT are crystalline and are predominantly oriented edge-on to the substrate, but the $PC_{71}BM$ is in the amorphous state. In the blend film, the diffractions for the lamellar structure ((300) and (400) peaks), for the π-π stacking and for the c-direction order became very weak; suggesting the presence of $PC_{71}BM$ suppressed the crystallization of PTh_4FBT. Because crystalline areas provide high diffraction contrast under the TEM observation,[42] the large and darker domains in the TEM image shown in **Figure 6a** were assigned as the crystalline PTh_4FBT domains. These large segregated polymer domains was not observed in the non-fluorinated analogues of PTh_4FBT studied by Chen and coworkers.[43] Moreover, the order along the c-direction was also absent in these non-fluorinated analogues at their pristine state. Thus, the cause of the strong segregation in the PTh_4FBT:$PC_{71}BM$ thin film can be attributed to the strong crystalline nature, and the more ordered solid-state packing of PTh_4FBT.

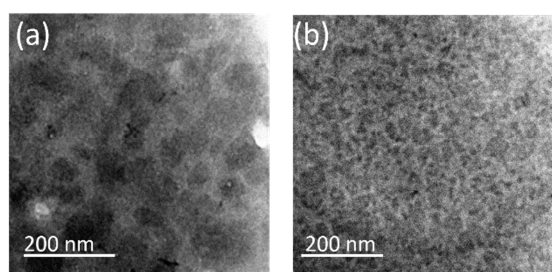

Figure 6. TEM images of PTh_4FBT:$PC_{71}BM$ thin films peprepared (a) without 1-CN, and (b) with 8 v% 1-CN.

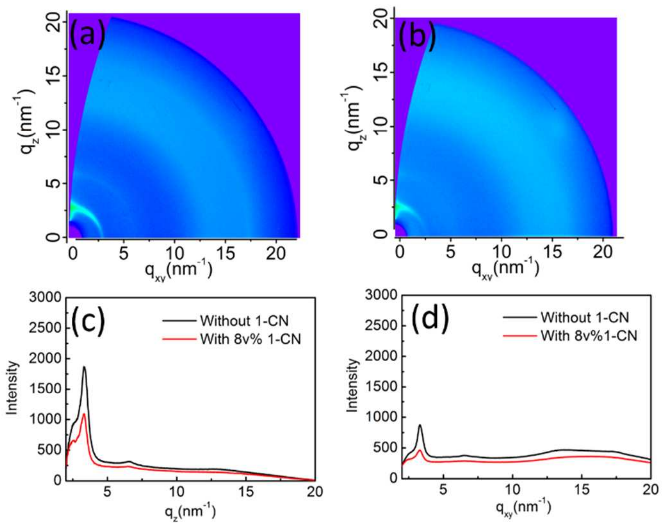

Figure 7. GI WAXS patterns of $PTh_4FBT:PC_{71}BM$ thin films peprepared (a) without 1-CN, and (b) with 8 v% 1-CN. (c) out-of-plane and (d) in-plane scans of the GI WAXS patterns.

Addition of 8 v% of 1-CN as a process additive further reduced the diffraction intensity and crystallinity of PTh_4FBT, as shown in **Figure 7b** and **7d**. In addition, in **Figure 6b**, the large dark domains were not observed in the films prepared with 1-CN, suggesting the decrease in the PTh_4FBT crystallinity was accompanied with the shrinkage of the darker crystalline PTh_4FBT domains. Thus, the addition of 1-CN reduces the crystallinity of PTh_4FBT and suppresses the phase separation in the blend thin film. The morphological change caused by the 1-CN additive significantly improved the device performance. The inverted BHJ PSCs of $PTh_4FBT:PC_{71}BM$ prepared with 8 v% of 1-CN delivered an averaged PCE of 7.75 % with V_{oc} of 0.76 V, a J_{sc} of 14.36 mA/cm^2, and a FF of 71.0 % under 100 mW/cm^2 AM 1.5 illumination (**Figure 8**, **Table 1**). Compared to the device fabricated without 1-CN, the reduced aggregation domain sizes, improved the J_{sc}, FF and therefore the PCE of the device.

Conclusions

In this study, the crystal structure of Th_2FBT and molecular model PTh_4FBT was analyzed. The conformational disorder in the crystalline phase of Th_2FBT confirmed that Th_2FBT has low conformational preference, and neither the inter-aryl S…F nor the CH…F interactions is sufficient to lock the conformation. In the case of PTh_4FBT, structural characterizations indicated that the diffraction pattern generated from the lattice containing PTh_4FBT with *anti*-conformation and zero interchain *c*-shift match best with the experimental 2D WAXS pattern. TEM and GI WAXD results showed that the strong crystalline nature of PTh_4FBT causes large aggregation domains in the $PTh_4FBT/PC_{71}BM$ thin film. Addition of 8 v% 1-CN additive decreased the aggregation size, and improved the J_{sc} and FF of the $PTh_4FBT:PC_{71}BM$ PSCs. The single-junction $PTh_4FBT/PC_{71}BM$ inverted PSCs delivered a high PCE of 7.75 % with V_{oc} of 0.76 V, a J_{sc} of 14.36 mA/cm^2, and a FF of 71.0 %.

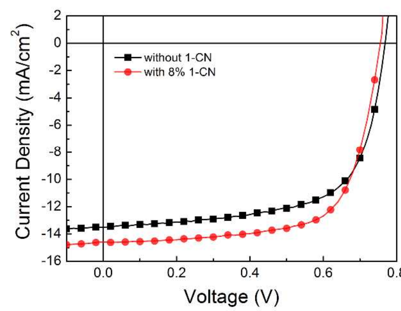

Figure 8. Current density-voltage characteristics of the $PTh_4FBT:PC_{71}BM$ based inverted BHJ PSCs processed with and without 8 v% of 1-CN under illumination of AM 1.5 G at 100 mW/cm^2.

Table 1. The device characteristics of $PTh_4FBT:PC_{71}BM$ BHJ PSCs. The values in parenthesis are the averaged values of eight devices.

$PTh_4FBT:PC_{71}BM$ (1:1)	V_{oc} [V]	J_{sc} [mA/cm^2]	FF [%]	PCE [%]
without 1-CN[a]	0.77	13.51	66	6.82
with 1-CN	0.76 (0.76)	14.36 (14.38)	71 (67)	7.75 (7.31)

[a]Values from reference.[12]

Acknowledgements

This work is supported by the Ministry of Science and Technology, Taiwan (NSC 100-2221-E-009 -152 -MY3) and "ATP" of the National Chiao Tung University and Ministry of Education, Taiwan. The authors thank the National Synchrotron Radiation Research Center (NSRRC) in Taiwan for assistance with the XRD measurements.

Notes and references

[a]Department of Applied Chemistry, National Chiao Tung University, 1001 Ta Hsueh Road Hsin-Chu, 30010 (Taiwan)
*E-mail: kclwang@nctu.edu.tw
[b]National Synchrotron Radiation Research Center, 101 Hsin-Ann Road, Hsinchu Science Park, Hsinchu, 300, Taiwan
Electronic Supplementary Information (ESI) available: The three possible conformations of Th_2FBT, detailed crystallographic data of Th_2FBT and *d*-spacing values of the PTh_4FBT crystal lattice can be found in Supporting Information. See DOI: 10.1039/b000000x/

1. Z. Chen, M. J. Lee, R. Shahid Ashraf, Y. Gu, S. Albert-Seifried, M. Meedom Nielsen, B. Schroeder, T. D. Anthopoulos, M. Heeney, I. McCulloch and H. Sirringhaus, *Adv. Mater.*, 2012, **24**, 647-652.
2. J. Fan, J. D. Yuen, W. Cui, J. Seifter, A. R. Mohebbi, M. Wang, H. Zhou, A. Heeger and F. Wudl, *Adv. Mater.*, 2012, **24**, 6164-6168.

3. H. Chen, Y. Guo, G. Yu, Y. Zhao, J. Zhang, D. Gao, H. Liu and Y. Liu, *Adv. Mater.*, 2012, **24**, 4618-4622.
4. I. Osaka, T. Kakara, N. Takemura, T. Koganezawa and K. Takimiya, *J. Am. Chem. Soc.*, 2013, **135**, 8834-8837.
5. K. H. Hendriks, G. H. Heintges, V. S. Gevaerts, M. M. Wienk and R. A. Janssen, *Angew. Chem. Int. Ed. Engl.*, 2013, **52**, 8341-8344.
6. Z. He, C. Zhong, S. Su, M. Xu, H. Wu and Y. Cao, *Nature Photon.*, 2012, **6**, 593-597.
7. S. Liu, K. Zhang, J. Lu, J. Zhang, H. L. Yip, F. Huang and Y. Cao, *J. Am. Chem. Soc.*, 2013, **135**, 15326-15329.
8. X. Guo, N. Zhou, S. J. Lou, J. Smith, D. B. Tice, J. W. Hennek, R. P. Ortiz, J. T. L. Navarrete, S. Li, J. Strzalka, L. X. Chen, R. P. H. Chang, A. Facchetti and T. J. Marks, *Nature Photon.,* 2013, **7**, 825-833.
9. H. N. Tsao, D. M. Cho, I. Park, M. R. Hansen, A. Mavrinskiy, Y. Yoon do, R. Graf, W. Pisula, H. W. Spiess and K. Mullen, *J. Am. Chem. Soc.*, 2011, **133**, 2605-2612.
10. N. E. Jackson, B. M. Savoie, K. L. Kohlstedt, T. J. Marks, L. X. Chen and M. A. Ratner, *Macromolecules*, 2014, **47**, 987-992.
11. X. Zhang, L. J. Richter, D. M. DeLongchamp, R. J. Kline, M. R. Hammond, I. McCulloch, M. Heeney, R. S. Ashraf, J. N. Smith, T. D. Anthopoulos, B. Schroeder, Y. H. Geerts, D. A. Fischer and M. F. Toney, *J. Am. Chem. Soc.*, 2011, **133**, 15073-15084.
12. J. F. Jheng, Y. Y. Lai, J. S. Wu, Y. H. Chao, C. L. Wang and C. S. Hsu, *Adv. Mater.*, 2013, **25**, 2445-2451.
13. L. Yang, J. R. Tumbleston, H. Zhou, H. Ade and W. You, *Energy Environ. Sci.,* 2013, **6**, 316.
14. A. C. Stuart, J. R. Tumbleston, H. Zhou, W. Li, S. Liu, H. Ade and W. You, *J. Am. Chem. Soc.*, 2013, **135**, 1806-1815.
15. H. Zhou, L. Yang, A. C. Stuart, S. C. Price, S. Liu and W. You, *Angew. Chem. Int. Ed. Engl.*, 2011, **50**, 2995-2998.
16. D. Niedzialek, V. Lemaur, D. Dudenko, J. Shu, M. R. Hansen, J. W. Andreasen, W. Pisula, K. Mullen, J. Cornil and D. Beljonne, *Adv. Mater.*, 2013, **25**, 1939-1947.
17. R. Rieger, D. Beckmann, A. Mavrinskiy, M. Kastler and K. Müllen, *Chem. Mater.*, 2010, **22**, 5314-5318.
18. G. Zuo, Z. Li, M. Zhang, X. Guo, Y. Wu, S. Zhang, B. Peng, W. Wei and J. Hou, *Polym. Chem.*, 2014, **5**, 1976.
19. I. Osaka, M. Shimawaki, H. Mori, I. Doi, E. Miyazaki, T. Koganezawa and K. Takimiya, *J. Am. Chem. Soc.*, 2012, **134**, 3498-3507.
20. T.-H. Lee, K.-Y. Wu, T.-Y. Lin, J.-S. Wu, C.-L. Wang and C.-S. Hsu, *Macromolecules*, 2013, **46**, 7687-7695.
21. T. Lei, Y. Cao, X. Zhou, Y. Peng, J. Bian and J. Pei, *Chem. Mater.*, 2012, **24**, 1762-1770.
22. T. Lei, J. H. Dou and J. Pei, *Adv. Mater.*, 2012, **24**, 6457-6461.
23. L. Ying, B. B. Hsu, H. Zhan, G. C. Welch, P. Zalar, L. A. Perez, E. J. Kramer, T. Q. Nguyen, A. J. Heeger, W. Y. Wong and G. C. Bazan, *J. Am. Chem. Soc.*, 2011, **133**, 18538-18541.
24. Y. Olivier, D. Niedzialek, V. Lemaur, W. Pisula, K. Mullen, U. Koldemir, J. R. Reynolds, R. Lazzaroni, J. Cornil and D. Beljonne, *Adv. Mater.*, 2014, **26**, 2119-2136.
25. N. C. Miller, E. Cho, M. J. Junk, R. Gysel, C. Risko, D. Kim, S. Sweetnam, C. E. Miller, L. J. Richter, R. J. Kline, M. Heeney, I. McCulloch, A. Amassian, D. Acevedo-Feliz, C. Knox, M. R. Hansen, D. Dudenko, B. F. Chmelka, M. F. Toney, J. L. Bredas and M. D. McGehee, *Adv. Mater.*, 2012, **24**, 6071-6079.
26. C. V. Hoven, X. D. Dang, R. C. Coffin, J. Peet, T. Q. Nguyen and G. C. Bazan, *Adv. Mater.*, 2010, **22**, E63-66.
27. H.-C. Liao, C.-S. Tsao, Y.-T. Shao, S.-Y. Chang, Y.-C. Huang, C.-M. Chuang, T.-H. Lin, C.-Y. Chen, C.-J. Su, U. S. Jeng, Y.-F. Chen and W.-F. Su, *Energy Environ. Sci.*, 2013, **6**, 1938.
28. J. Peet, J. Kim, N. E. Coates, W. L. Ma, D. Moses, A. J. Heeger and G. C. Bazan, *Nat. Mater.*, 2007, **6**, 497-500.
29. J. K. Lee, W. L. Ma, C. J. Brabec, J. Yuen, J. S. Moon, J. Y. Kim, K. Lee, G. C. Bazan and A. J. Heeger, *J. Am. Chem. Soc.*, 2008, **130**, 3619-3623.
30. P. M. Beaujuge, H. N. Tsao, M. R. Hansen, C. M. Amb, C. Risko, J. Subbiah, K. R. Choudhury, A. Mavrinskiy, W. Pisula, J. L. Bredas, F. So, K. Mullen and J. R. Reynolds, *J. Am. Chem. Soc.*, 2012, **134**, 8944-8957.
31. M. Brinkmann, E. Gonthier, S. Bogen, K. Tremel, S. Ludwigs, M. Hufnagel and M. Sommer, *ACS Nano*, 2012, **6**, 10319-10326.
32. Z. Chen, P. Cai, J. Chen, X. Liu, L. Zhang, L. Lan, J. Peng, Y. Ma and Y. Cao, *Adv. Mater.*, 2014, **26**, 2586-2591.
33. N. E. Jackson, B. M. Savoie, K. L. Kohlstedt, M. Olvera de la Cruz, G. C. Schatz, L. X. Chen and M. A. Ratner, *J. Am. Chem. Soc.*, 2013, **135**, 10475-10483.
34. J. Zapala, M. Knor, T. Jaroch, A. Maranda-Niedbala, E. Kurach, K. Kotwica, R. Nowakowski, D. Djurado, J. Pecaut and M. Zagorska, *Langmuir*, 2013, **29**, 14503-14511.
35. C. L. Donley, J. Zaumseil, J. W. Andreasen, M. M. Nielsen, H. Sirringhaus, R. H. Friend and J.-S. Kim, *J. Am. Chem. Soc.*, 2005, **127**, 12890-12899.
36. W. Ma, C. Yang, X. Gong, K. Lee and A. J. Heeger, *Adv. Funct. Mater.*, 2005, **15**, 1617-1622.
37. Y.-J. Cheng, C.-H. Hsieh, P.-J. Li and C.-S. Hsu, *Adv. Funct. Mater.*, 2011, **21**, 1723-1732.
38. J. S. Moon, C. J. Takacs, S. Cho, R. C. Coffin, H. Kim, G. C. Bazan and A. J. Heeger, *Nano Lett.*, 2010, **10**, 4005-4008.
39. H.-C. Liao, C.-C. Ho, C.-Y. Chang, M.-H. Jao, S. B. Darling and W.-F. Su, *Mater. Today*, 2013, **16**, 326-336.
40. H. Bronstein, J. M. Frost, A. Hadipour, Y. Kim, C. B. Nielsen, R. S. Ashraf, B. P. Rand, S. Watkins and I. McCulloch, *Chem. Mater.*, 2013, **25**, 277-285.
41. T. Lei, X. Xia, J. Y. Wang, C. J. Liu and J. Pei, *J. Am. Chem. Soc.*, 2014, **136**, 2135-2141.
42. D. B. Williams and C. B. Carter, *Transmission Electron Microscopy*, Springer, 2nd edn., 2009, pp. 381-386.
43. K.-H. Ong, S.-L. Lim, J. Li, H.-K. Wong, H.-S. Tan, T.-T. Lin, L. C. H. Moh, J. C. de Mello and Z.-K. Chen, *Polym. Chem.*, 2013, **4**, 1863.

TABLE OF CONTENTS

Structural analysis of PTh_4FBT suggested the high crystalline nature of PTh_4FBT relates to its zero *c*-shift co-facially packing.

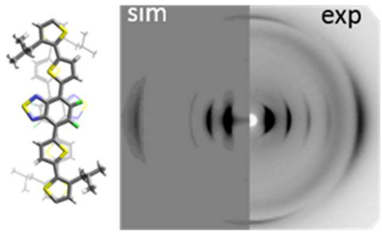

Assembled with **zero *c*-shift** and ***anti*-conformation**.